JOURNAL OF GEOPHYSICAL RESEARCH, VOL. 115, C05022, doi:10.1029/2009JC005734, 2010

Tropical Pacific Ocean and the Madden-Julian Oscillation: Role of wind and buoyancy forcing

Xu Zhang,[1] Youyu Lu,[2] Keith R. Thompson,[3] Jing Jiang,[1] and Hal Ritchie[4]

Received 19 August 2009; revised 7 January 2010; accepted 13 January 2010; published 27 May 2010.

[1] A global ocean circulation model is used to examine the dynamical response of the tropical Pacific Ocean to forcing associated with the Madden-Julian Oscillation (MJO). Model sensitivity experiments first reveal that MJO-related changes in sea level are caused primarily by changes in wind stress. Further, the MJO-related changes in sea surface temperature (SST) are mainly caused by buoyancy (heat) flux in the Indian Ocean, by wind stress in the central tropical Pacific, and by both buoyancy flux and wind stress in the eastern tropical Pacific. Additional model sensitivity studies quantify the tropical Pacific Ocean response to MJO wind forcing. The simulations reveal that the subsurface temperature variations associated with the MJO propagate eastward along the thermocline and rise to the surface in the eastern Pacific. Zonal advection plays a dominant role in SST variation in the central Pacific; vertical advection plays an important role in the evolution of subsurface and surface temperatures in the eastern Pacific. Finally, it is shown that MJO wind forcing can rectify SST variations through nonlinear interactions of the intraseasonal variations of the zonal currents and the zonal SST gradient.

Citation: Zhang, X., Y. Lu, K. R. Thompson, J. Jiang, and H. Ritchie (2010), Tropical Pacific Ocean and the Madden-Julian Oscillation: Role of wind and buoyancy forcing, *J. Geophys. Res.*, *115*, C05022, doi:10.1029/2009JC005734.

1. Introduction

[2] The Madden-Julian Oscillation (MJO) is the dominant mode of intraseasonal variability in the tropical atmosphere [*Madden and Julian*, 1994]. Its influence is widespread and can involve timescales beyond the intraseasonal band [e.g., *Hsu*, 1996]. In recent years, the interaction between the MJO and ocean has received increasing attention because of the need to understand the dynamics controlling the predictability of both weather and climate.

[3] In the warm pool region of the Indo-Pacific, where the MJO signals are the strongest, the MJO disturbs the ocean by modifying surface fluxes of momentum, heat, and freshwater [e.g., *Jones et al.*, 1998; *Shinoda et al.*, 1998]. Intraseasonal perturbations in ocean temperature, salinity, and currents in the mixed layer have been observed [e.g., *Zhang and McPhaden*, 2000]. Numerical models have also been used to better understand the ocean response to the MJO in the warm pool region [e.g., *Shinoda and Hendon*, 2001; *Waliser et al.*, 2003].

[4] In the central and eastern Pacific, the ocean response to remote MJO forcing is observed in changes of sea level, thermocline depth, currents, and sea surface temperature (SST). Using the observational data from the Tropical Atmosphere-Ocean buoy array, *Zhang* [2001] identified equatorially elongated, intraseasonal perturbations in SST in the eastern Pacific that are coherent with the vertical temperature gradient of the upper ocean. He then hypothesized a link between the SST changes and MJO-forced equatorial Kelvin waves. According to Zhang's hypothesis, downwelling (upwelling) Kelvin waves are generated by strong MJO westerly (easterly) in the western Pacific; the waves propagate into the eastern Pacific and suppress (lift) the thermocline; thus, the vertical advection and vertical temperature gradient are altered, and warm (cool) SST anomalies are induced.

[5] One important implication of MJO-ocean interaction is the possibility that the MJO might influence the El Nino-Southern Oscillation (ENSO) [*Zhang and Gottschalck*, 2002]. In previous studies, it has been proposed that the MJO acts as a disruptive or stochastic influence on an otherwise regular ENSO cycle, thereby contributing to the observed irregularity of ENSO [e.g., *Moore and Kleeman*, 1999]. The rectification of the MJO on interannual timescales and the influence of the MJO on the mean state of the ocean have also been investigated. For example, *Kessler and Kleeman* [2000] addressed the rectification of the MJO into the ENSO cycle in the western Pacific.

[6] In this study, we explore the response of the tropical Pacific Ocean to MJO forcing using an ocean general circulation model and realistic surface forcing. The first objective is to assess the relative importance of the surface momentum (wind stress) and buoyancy fluxes in causing the

[1]School of Atmospheric Sciences, Nanjing University, Nanjing, China.
[2]Ocean Sciences Division, Fisheries and Oceans Canada, Bedford Institute of Oceanography, Dartmouth, Nova Scotia, Canada.
[3]Department of Oceanography, Dalhousie University, Halifax, Nova Scotia, Canada.
[4]Meteorological Research Division, Environment Canada, Dorval, Quebec, Canada.

0148-0227/10/2009JC005734

MJO-related changes in sea level and SST. This is achieved by model sensitivity experiments in which either the surface momentum or the buoyancy fluxes are set to climatology. The second objective is to explore the mechanisms relating the changes of temperature (including SST) in the tropical Pacific to MJO wind forcing. The contribution of zonal and vertical advection in the temperature budget is quantified, and the aforementioned hypothesis of *Zhang* [2001] concerning SST changes in the eastern Pacific is tested. Finally, we quantify the SST changes due to the rectification of MJO forcing.

[7] In section 2, we review the observations, ocean model, and experiment setup. In section 3, on the basis of observations and model solutions, we describe the MJO-related sea level and SST changes and assess the relative importance of surface momentum and buoyancy fluxes. In section 4, the model results are analyzed in order to better understand the mechanisms controlling SST variations due to the MJO wind forcing. The temporal-spatial structure of the associated ocean circulation and temperature changes is described, and the contributions from the zonal and vertical advections to the temperature tendency budget are evaluated. Section 5 provides a summary, a discussion, and questions for further study.

2. Observations and Model Experiments

2.1. Ocean Observations and the MJO Index

[8] The observational data sets used for model validation are the (1) weekly mean, optimally interpolated SST (OISST) product of *Reynolds and Smith* [1994], and (2) the weekly mean, gridded sea level anomalies from the TOPEX/POSEIDON altimeter measurements obtained from the Archiving, Validation, and Interpretation of Satellite Oceanographic (AVISO) Web site (http://www.aviso.oceanobs.com). The MJO is represented by the bivariate index of *Wheeler and Hendon* [2004], obtained from the Web site of the Australia Bureau of Meteorology (http://www.bom.gov.au). The MJO index is based on the first two empirical orthogonal functions (EOFs) calculated from multivariate fields including the equatorially averaged 850 hPa zonal wind, 200 hPa zonal wind, and outgoing long-wave radiation observed by satellites. The first two EOFs are referred to as the real-time multivariate MJO series 1 and 2 and denoted by RMM1 and RMM2, respectively. We note that while the variations of the RMM1 and RMM2 are dominated by the MJO signals, they also include contributions from other atmospheric waves, such as equatorial Rossby waves and convective Kelvin waves [*Roundy et al.*, 2009]. Note the use of only the first two principal components may exclude an eastward extending mode of wind variability [*Kessler*, 2001].

2.2. Ocean Model

[9] The global ocean general circulation model used in this study is based on version 2.3 of Nucleus for European Modeling of the Ocean (NEMO) which includes an ocean component [*Madec et al.*, 1998] and sea ice module [*Fichefet and Morales Maqueda*, 1997]. The model grids follow the tripolar configurations that are widely used for global ocean modeling [e.g., *Barnier et al.*, 2006]. The horizontal grid has a nominal resolution of 1° in longitude/latitude, with a meridional refinement within 10° of the equator. Within this refinement zone, the grid size reaches a maximum of 120 km in the zonal direction and a minimum of 35 km in the meridional direction at the equator. Away from the refinement zone, the grid boxes are approximately square. The model's bathymetry is derived from version 9 of a global data set at 1 min spatial resolution (downloaded from http://topex.ucsd.edu/marine_topo), updated from *Smith and Sandwell* [1997]. There is a maximum of 46 levels in the vertical, with level thickness increasing from 6 m at the surface to 200 m at a depth of 1750 m and increasing to a maximum of 250 m at the bottom of the deep basins. The maximum depth represented in the model is 5720 m. Vertical eddy diffusivity and viscosity coefficients are computed using an order of 1.5 turbulent closure scheme based on a prognostic equation for the turbulent kinetic energy [*Blanke and Delecluse*, 1993]. Horizontal mixing of momentum is parameterized by biharmonic diffusion with the viscosity coefficient varying in proportion to the third power of grid spacing. Its maximum value is -2.5×10^{13} m^4 s^{-1}. Eddy-induced tracer advection and along-isopycnal diffusion are parameterized following *Gent and McWilliams* [1990] with the mixing coefficient set at 1000 m^2 s^{-1}.

[10] The model is driven by a recently compiled atmospheric forcing data set created for the Common Ocean-ice Reference Experiment (CORE), a corrected version of the reanalysis fields from the U.S. National Center for Environmental Prediction [*Large and Yeager*, 2004]. Input fields include the 6 hourly values of air temperature, wind and humidity at 10 m height, daily short- and long-wave radiation, and total precipitation (rain plus snow). The turbulent heat and momentum fluxes are computed using the bulk formulae available in NEMO 2.3. The runoff of major rivers is specified according to a monthly climatology compiled by *Barnier et al.* [2006]. No surface restoring to the sea surface temperature is applied. However, the model's sea surface salinity is restored to its monthly climatology with a 15 day restoring time scale.

2.3. Model Experiments

[11] The model is first run for 10 years using the "normal year forcing" (NYF) of CORE, which represents the climatology of the reanalysis period. This spin-up simulation is initialized with the January climatology of temperature and salinity and the associated geostrophic velocities. Following the spin-up, a control simulation (CTL) is performed using version 1 of the CORE forcing covering the period 1958–2004. At the end of 1989, the state variables of the CTL run are saved in order to initialize three sensitivity simulations for the period 1990–2004. The first sensitivity study is referred to as BUOY, which is the same as CTL except that the wind stress is calculated using the 10 m wind velocities from the climatology of NYF. The second is referred to as WIND, which is the same as CTL except that the input atmospheric variables for computing the surface buoyancy (heat and freshwater) fluxes are taken from the climatology of NYF. The third run is denoted as MJO, which is the same as BUOY except that the wind stress is calculated using the combined 10 m climatological plus the reconstructed MJO winds (see Appendix A for details). The model experiments, the input variables for surface forcing, and the notation of variables being analyzed are summarized Table 1.

Table 1. Model Experiments, Input Variables for Computing Surface Forcing, and the Notation of Variables Being Analyzed[a]

Model Experiments	Inputs for Computing Wind Stress	Inputs for Computing Buoyancy Flux	Variables Analyzed
CTL	U, V	full	η_c, T_c
BUOY	U_c, V_c	full	η_b, T_b, u_b, w_b
WIND	U, V	climatology	η_w, T_w
MJO	$U_c + U_m$, V_c	full	η_m, T_m, u_m, w_m

[a]U and V denote the zonal and meridional components of the full CORE wind; U_c and V_c are the climatological winds of NYF; and U_m is the zonal wind coherent with the MJO; η, T, u, and w represent sea level, temperature, zonal ocean velocity, and vertical ocean velocity, respectively; the subscripts "c," "b," "w," and "m" denote the CTL, BUOY, WIND, and MJO runs, respectively.

[12] For all four model simulations, 5 day averaged fields for 1990–2004 are saved in order to evaluate the ocean response to MJO forcing.

3. Relative Importance of Surface Momentum and Buoyancy Fluxes

[13] On the basis of observations and the results from the CTL, BUOY, and WIND runs, we examine the sea level and SST changes related to the MJO. For the weekly time series of sea level and SST at a specific location, a high-pass filter with a cutoff period of 120 days is first applied to suppress energy at periods longer than intraseasonal. The daily time series of the two MJO indices are averaged into weekly means (in accord with the sea level and SST observations). The following coherency analysis method, as described by *Zhang et al.* [2009] and *Oliver and Thompson* [2010], is then applied. The power spectral density ($f(\omega)$, where ω is frequency) and the squared multiple coherence ($k^2(\omega)$) between the variable of interest at a given grid point and the two MJO indices are computed. An overall measure of the variance associated with the MJO is given by integrating the squared coherence multiplied by the spectral density at all frequencies: $\sigma^2 = \int k^2(\omega) f(\omega)\, d\omega$. Time series of the MJO-related sea level and SST changes are obtained by applying the inverse Fourier transformation, the same technique described in Appendix A for extracting the MJO-related zonal wind.

[14] Differencing the sea level fields from the MJO and BUOY runs gives a sea level signal that is mainly related to the MJO. However, the difference of the SST fields from the MJO and BUOY runs contains a significant component that is unrelated to the MJO. This component is induced primarily by stochastic tropical instability waves (TIWs) and is removed by the coherency analysis described above. In the tropical Pacific, the TIWs can be amplified because downwelling Kelvin waves accelerate the Equatorial Undercurrent (EUC) thus increasing the shear between the EUC and the South Equatorial Current [*Giese and Harrison*, 1991].

3.1. Sea Level

[15] Numerous earlier studies have shown that the tropical oceans behave in many ways as a two-layer fluid, with thermocline variations reflected in sea level changes. In a

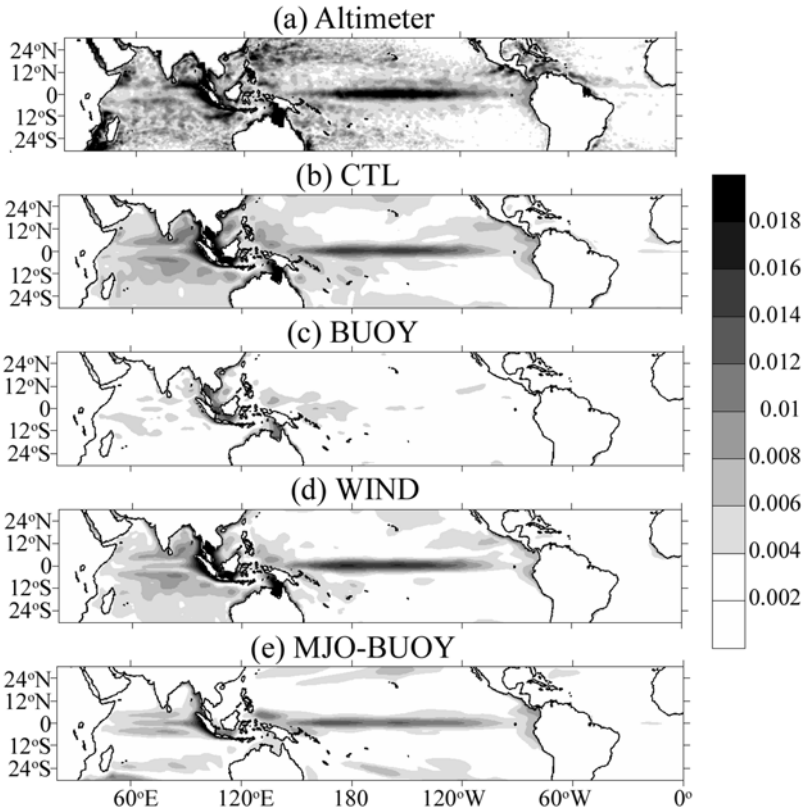

Figure 1. Standard deviation of sea level variations (in m) coherent with the MJO, derived from (a) altimeter observations and the simulations of (b) η_c, (c) η_b, (d) η_w, and (e) $\eta_m - \eta_b$.

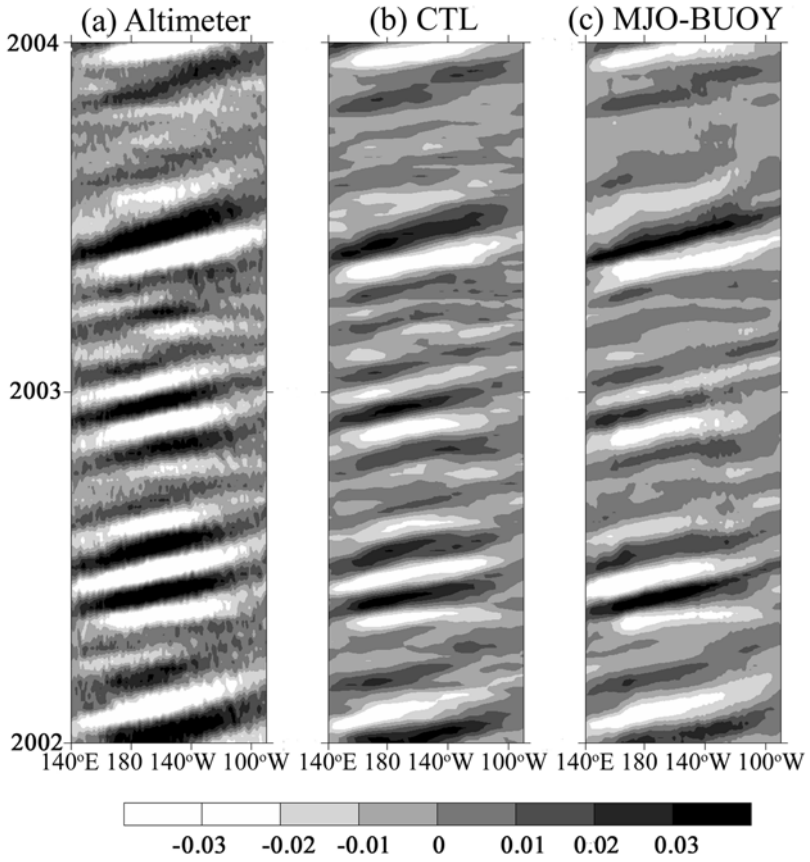

Figure 2. Longitude-time variations of sea level coherent with the MJO (in m) at the equator during 2002–2003, derived from (a) altimeter observations, (b) η_c, and (c) $\eta_m - \eta_b$.

recent study, *Zhang et al.* [2009] showed that the MJO-related sea level changes in the tropical Pacific can be described quite accurately using simple, wind-forced linear Kelvin wave dynamics. Thus, examining the sea level changes can help to check the realism of the more complex NEMO model through its ability to reproduce wind-forced Kevin waves.

[16] Figure 1 maps the standard deviation of sea level related to the MJO, derived from altimeter observations and model solutions. The results from the CTL, BUOY, WIND, and MJO runs are denoted as η_c, η_b, η_w, and η_m, respectively. The comparison shows that the CTL run, forced with the full surface momentum and buoyancy fluxes from the CORE data set, can produce realistic simulations of the sea level variability in the tropical Pacific and eastern Indian Ocean (compare Figures 1a and 1b). In the tropical Pacific the CTL run underestimates the variability possibly due to model error or the accuracy of the reanalysis forcing. Further, with surface buoyancy forcing set to climatology, the WIND run gives a solution that is quite similar to the CTL run at low latitudes (Figure 1d). This suggests that wind stress is the dominant forcing for MJO-related sea level changes in the study area. Indeed, with wind stress set to climatology, the BUOY run predicts insignificant sea level variations associated with the MJO (Figure 1c).

[17] Finally, Figure 1e shows that $\eta_m - \eta_b$ captures most of the elevated sea level variability near the equator, with slightly reduced magnitudes compared with η_c and η_w. This suggests that MJO-related zonal wind variations are the primary forcing for the equatorial Kelvin waves. In the Indian Ocean, elevated standard deviations appear along the equator and two off-equatorial bands. The variations along the off-equatorial bands can be related to the reflection of equatorial Kelvin waves into Rossby waves at the eastern boundary of the basin. The reflection signals of the Kelvin waves can be found at the eastern boundary of the Pacific Ocean as well. Sea level signals can also propagate poleward along the coasts of North America and South America [*Enfield and Lukas*, 1983].

[18] Wave propagation is clearly evident in the longitude-time plots of MJO-related sea level variations during 2002–2003 derived from observations, η_c, and $\eta_m - \eta_b$ (Figure 2). The MJO-related westerly winds generate the downwelling Kelvin waves, and the easterly winds generate the upwelling Kelvin waves. The phase speeds of the Kelvin waves, from model and observations, are about 3.3 m s^{-1} and clearly consistent with each other. The above comparisons illustrate that the difference between the MJO and BUOY runs can capture well the MJO-forced sea level variations forced by the MJO wind, although they moderately underestimate their magnitudes.

3.2. Sea Surface Temperature

[19] The same methods used to analyze the sea level variations are also used to estimate the SST variations coherent with the MJO. Figure 3 shows maps of the standard

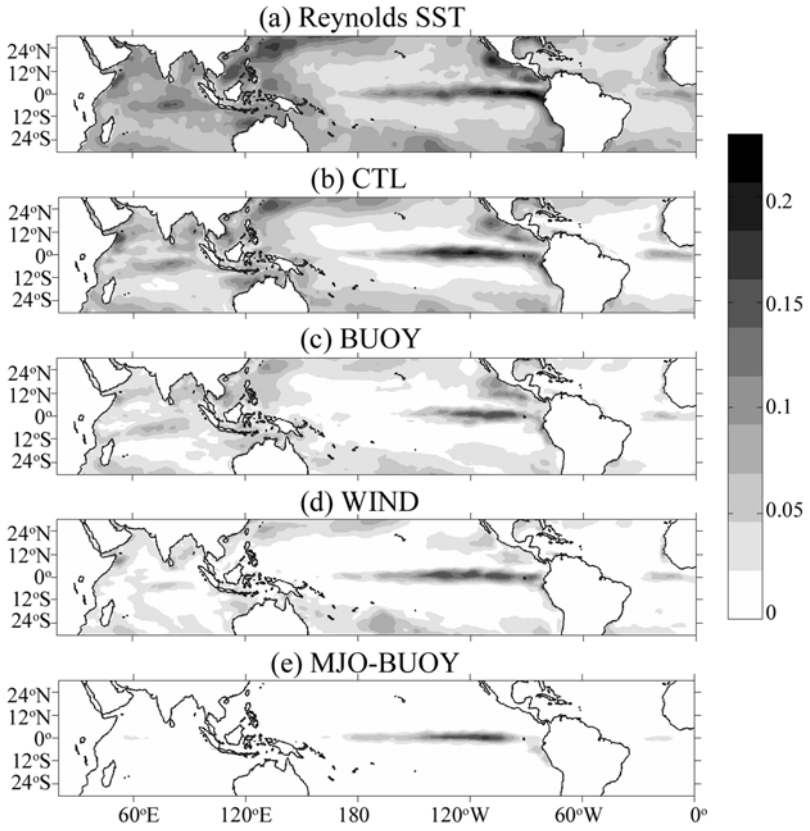

Figure 3. Standard deviation of SST (in °C) coherent with the MJO, derived from (a) the optimally interpolated SST (OISST) data set and the model simulations of (b) T_c, (c) T_b, (d) T_w, and (e) $T_m - T_b$. Note an additional coherence analysis is applied to $T_m - T_b$ (see text for details).

deviation of SST derived from the OISST data set and the model solutions. The results from the CTL, BUOY, WIND, and MJO runs are denoted as T_c, T_b, T_w, and T_m, respectively. On the basis of both observations and the CTL run, significant variations are found in the central and eastern equatorial Pacific, the northeastern and northwestern Pacific, and the Indian Ocean. The CTL run predicts weaker SST variability in the far eastern tropical Pacific, compared to observations. With only realistic buoyancy forcing, the BUOY run predicts elevated SST variability in the Indian Ocean. The main components in the buoyancy forcing are variations in radiation and latent heat fluxes [*Hendon*, 2005]. In the eastern tropical Pacific, the roles played by buoyancy forcing and wind stress are comparable. In the central tropical Pacific, the impact of wind stress variations is more important than buoyancy forcing.

[20] Figure 3e shows the standard deviation of the variations of $T_m - T_b$ that are coherent with the MJO. (Figure 3e is based on results from the coherency approach described above.) Elevated magnitudes of $T_m - T_b$ are only found in the central and eastern equatorial Pacific. In the Indian Ocean, there is no apparent SST variation associated with the MJO wind. This may be due to the difference in the background thermocline structure in the Indian and Pacific oceans. The differences in background conditions can have a large impact on ocean response [*Kessler*, 2005].

[21] Figure 4 shows longitude-time sections of SST coherent with the MJO derived from observations and $T_m - T_b$. The model-simulated changes agree well with observations, although the predicted magnitudes are smaller in the far eastern Pacific. A closer look reveals that in the eastern basin, some eastward propagating signals in the observations are missed in the model solutions. This model deficiency needs further study. In the eastern Pacific, downwelling Kelvin waves produce positive SST anomalies, and the upwelling Kelvin waves produce negative anomalies, with magnitudes of 0.2°C to 0.5°C. The anomalies of opposite signs tend to cancel each other out. These particular patterns have been observed by *Zhang* [2001], who related them to the effect of the MJO-forced Kelvin wave activity.

4. Physical Mechanisms Relating Temperature Variations to MJO Wind

[22] In this section, we analyze further the difference between the MJO and BUOY runs. The goal is to identify the physical mechanisms relating temperature changes to the MJO wind in the equatorial Pacific. Advection by currents plays a dominant role in the wind-induced temperature changes. Hence, the MJO wind-forced equatorial currents are described first.

4.1. Equatorial Currents

[23] Figure 5a shows the standard deviation of $u_m - u_b$ which represents the surface zonal currents forced by the MJO-related zonal wind. The largest variance of $u_m - u_b$

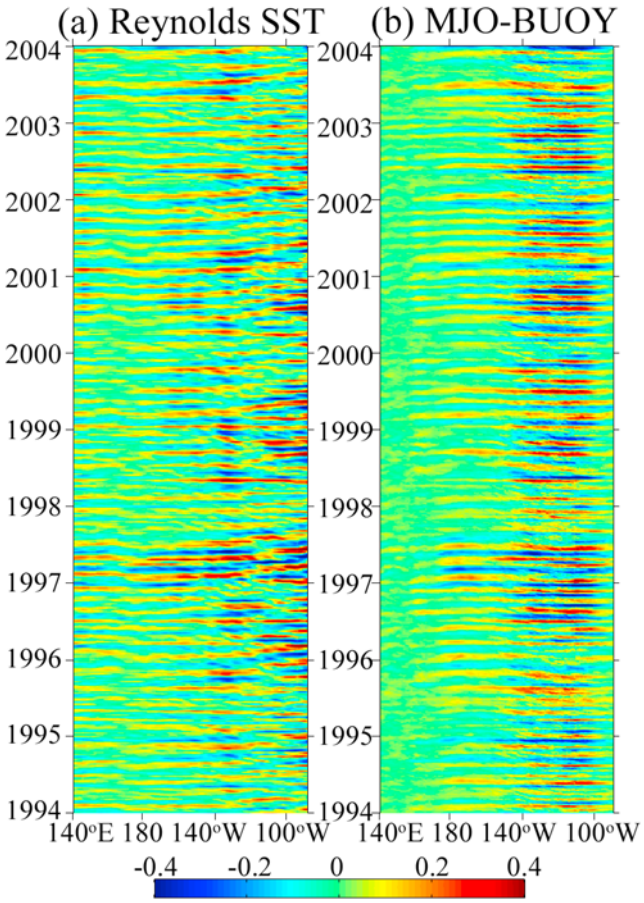

Figure 4. Longitude-time variations of SST coherent with the MJO (in °C) at the equator, derived from (a) the OISST data set and (b) $T_m - T_b$.

occurs in the eastern Indian and the western Pacific oceans, where the MJO winds are the strongest. The lower variance of $u_m - u_b$ in the western Indian Ocean is consistent with the finding of *Han et al.* [2001], who suggested that the intraseasonal current is forced by winds not associated with the MJO in this region. In the Pacific Ocean, $u_m - u_b$ is stronger to the west of the dateline than in the eastern basin.

[24] Longitude-time variations of $u_m - u_b$ at surface in the equatorial Pacific are shown in Figure 6a. Positive velocity anomalies are forced by westerly winds, and negative anomalies are forced by easterly winds. The reconstructed MJO winds retain the desired feature of the MJO that the westerly wind is usually much stronger than its easterly counterpart. Thus, the eastward currents tend to be stronger than the westward currents.

[25] In the warm pool of the western tropical Pacific, the zonal current variations are locally large but play a minimal role in causing SST variations because of the small horizontal SST gradients there [*Shinoda and Hendon*, 2001]. At the eastern edge of the warm pool, where horizontal SST gradients are large, zonal advection plays an important role in causing the SST variations. Westerly winds generate zonal currents that advect the east edge of the warm pool eastward, and easterly winds do the opposite. *Kessler and Kleeman* [2000] showed that even idealized MJO winds with equal-amplitude easterly and westerly winds can generate mean eastward currents. This is because the first-order nonlinear effect on the equatorial zonal currents is independent of wind direction [*Gill*, 1975]. The net effect of oscillating intraseasonal winds is to push the warm pool slowly eastward. Therefore, the MJO wind forcing can alter the mean state of the ocean and develop rectified low-frequency zonal current anomalies.

[26] Figure 6a also shows significant interannual variation in the magnitude of $u_m - u_b$ at the surface. During the ENSO warm events of 1997–1998 and 2002–2003, $u_m - u_b$ is stronger than that during the ENSO cold events of 1999–2000. The zonal advection of SST driven by surface zonal currents is thought to be important for the development of the ENSO. *Picaut et al.* [1997] proposed a conceptual advective-reflective oscillator model for ENSO. Using this model, they emphasized a positive feedback of zonal currents that advect the western Pacific warm pool toward the east.

[27] It should be noted that MJO-forced currents in the eastern Pacific are disturbed by variations associated with other internal processes (e.g., TIWs) not related to MJO wind forcing. In the central equatorial Pacific, the MJO-forced signals dominate the variation of the zonal currents.

[28] The MJO wind also causes significant variations of current at depth in the tropics, as illustrated by the standard deviation of $u_m - u_b$ and $w_m - w_b$ in the vertical section of the tropical Pacific shown in Figures 5b and 5c. Significant variations of zonal flow occur from the surface to about 100 m depth; the variations are strongest in the western basin and decrease gradually toward the eastern basin. The strongest variations in vertical flow occur at about 50 m depth. Unlike the zonal current, variations of the vertical flow in the eastern basin are not weak and have a magnitude similar to vertical currents in the western basin.

4.2. Role of Vertical and Zonal Advection

[29] To examine the temporal-vertical variation of temperature in the tropical Pacific, we calculated extended empirical orthogonal functions (EEOFs) [*Weare and Nasstrom*, 1982] of $T_m - T_b$. Figure 7 shows the first EEOF at selected lags. The first mode represents the response of the ocean to the westerly and easterly phases of the MJO. At zero lag, the pattern shows a near-surface warming in the eastern Pacific produced by a downwelling Kelvin wave associated with the westerly phase of the MJO. The warming signal is clearly evident in the SST. At the same time, a negative subsurface temperature anomaly associated with upwelling Kelvin wave appears in the western Pacific. At 1 month lag, the warming in the eastern Pacific decreases, while the negative subsurface temperature anomaly which originated in the western basin propagates eastward along the thermocline. Meanwhile, a positive temperature anomaly is generated by the westerly MJO wind in the western basin. At lags of 2 and 3 months, we can see the propagation and decay of the positive and negative anomalies. The subsurface temperature anomalies form in the western Pacific, propagate eastward along the thermocline, and rise to the surface in the eastern Pacific.

[30] Next we quantify the contributions of zonal and vertical advection to the temperature evolution using the solutions of the BUOY and MJO runs. The contribution of meridional advection has been discussed by *Waliser et al.*

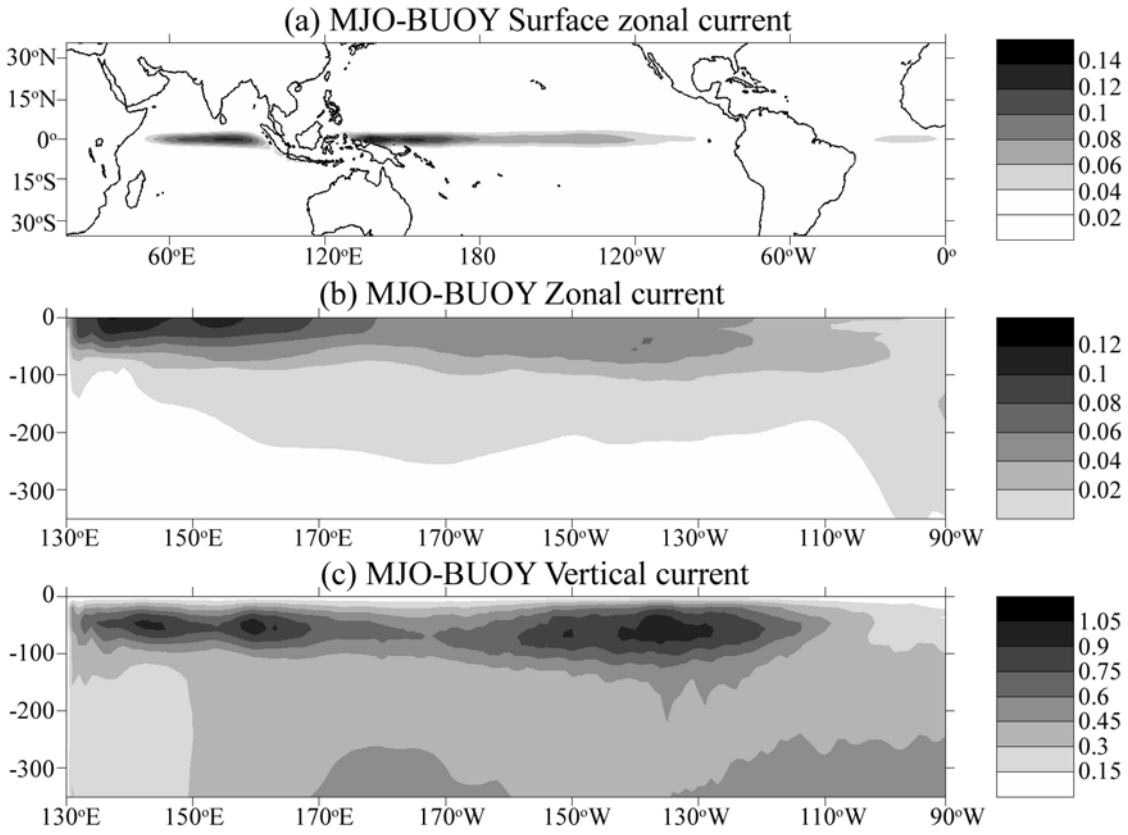

Figure 5. Standard deviation of (a) $u_m - u_b$ at surface (in m s^{-1}) and (b) $u_m - u_b$ (in m s^{-1}) and (c) $w_m - w_b$ (in 10^{-5} m s^{-1}) in the upper 350 m of the equatorial Pacific Ocean. Depths are in m.

[2003] and *Belamari et al.* [2003]. Figure 8 shows the standard deviation of the advection and the tendency terms obtained by differencing the respective terms from the MJO and BUOY runs, i.e., $u_m\partial T_m/\partial x - u_b\partial T_b/\partial x$, $w_m\partial T_m/\partial z - w_b\partial T_b/\partial z$, and $\partial(T_m - T_b)/\partial t$, in the vertical section along the equator. Although the enhanced TIW activity makes a contribution, the zonal advection effect shown in Figure 8 is mostly associated with the MJO-forced Kelvin waves. The zonal advection effect is significant in the eastern Pacific, where the most enhanced signals are confined near the surface. At a depth of 100 m, the relatively high zonal advection effect may be related to the amplification of the EUC. In the central Pacific, zonal advection plays a dominant role in SST changes but only accounts for a small part of the subsurface temperature variability (compare Figures 8a and 8c). The vertical advection is responsible for most of the subsurface temperature anomaly tendency, especially during its formation in the western basin and rising in the eastern basin (compare Figures 8b and 8c).

[31] The sea level and SST variations associated with the MJO differ significantly in their propagation patterns: sea level variations propagate eastward at a speed consistent with baroclinic Kelvin waves (Figure 2), while the SST anomalies are predominantly stationary. The physical processes responsible for these differences have been discussed by *McPhaden* [2002]. This study quantifies the intraseasonal SST variations along the equator associated with the zonal and vertical advection caused by the MJO wind forcing.

4.3. Rectification to Low Frequency

[32] From a linear point of view, the warming effect of the downwelling Kelvin waves is canceled by the cooling effect of the upwelling waves. Thus, any growing SST feature cannot be amplified and maintained for a protracted time, thereby allowing strong interaction with the atmosphere [*Zavala-Garay et al.*, 2008]. In reality, nonlinear effects can cause a transfer of energy from high to low frequencies. *Kessler and Kleeman* [2000] have suggested that this is important in the western and central Pacific.

[33] In a recent study by *Jiang et al.* [2009], rectification of SST variability to low frequency was quantified by the product of the intraseasonal zonal currents and the zonal gradient of intraseasonal SST. From our model results, this rectification can be represented by low-pass filtering the term $(u_m - u_b)\partial(T_m - T_b)/\partial x$. The longitude-time plot of this term is shown in Figure 6b. Smoothing with a 90 day running window has been applied in order to suppress signals on intraseasonal time scales. The rectification effect is noticeable in both the western and eastern Pacific. The signals are relatively large to the east of 150°W. In the western Pacific, the rectification is due mainly to the strong intraseasonal zonal currents; in the eastern Pacific, the rectification comes from the increased magnitude of the intraseasonal SST induced by Kelvin waves. The rectified signal shows clear interannual variability. During 1997–1998 and 2001–2004, relatively strong rectification is evident in both the eastern and western Pacific. The rectification sig-

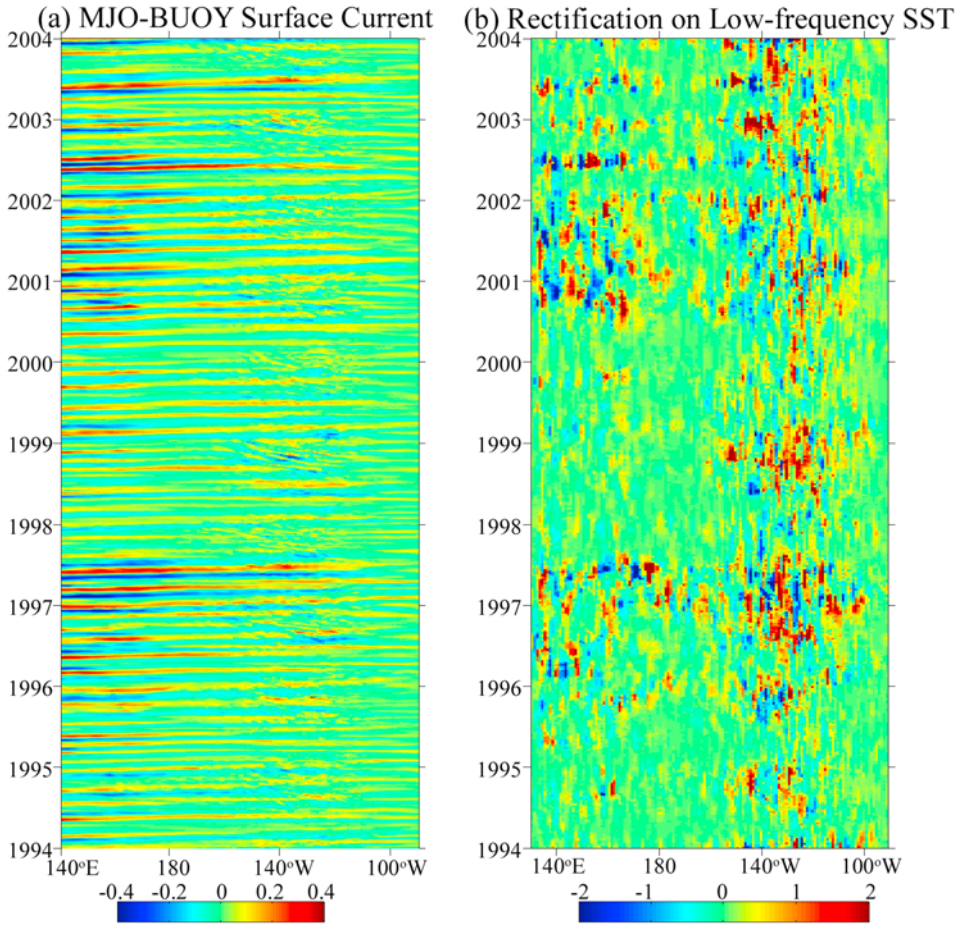

Figure 6. Longitude-time variations of (a) $u_m - u_b$ at surface (in m s^{-1}) and (b) the SST rectification term (in 10^{-8} °C s^{-1}) at the equator. The rectification is quantified by smoothing the $(u_m - u_b)\partial(T_m - T_b)/\partial x$ term with a 90 day running window.

nals were negligible in the western Pacific during 1993–1996 and 1998–2000, when the MJO activity was weak. Note that the interannual variations of the rectified SST signals are associated with the year-to-year variability in the amplitude of the MJO winds that are retained by our extraction procedure, even though the low-frequency wind variations are eliminated. These year-to-year variations should be interpreted as coming from atmospheric internal dynamics [*Slingo et al.*, 1999].

[34] The magnitude of rectification in the present solution is smaller than that of *Jiang et al.* [2009], who used QuikSCAT winds to force the ocean model. The underestimation in our solution may be related to the use of atmospheric reanalysis winds, which are consistently weaker than the QuikSCAT winds [*Gille*, 2005].

[35] The MJO wind may also contain variations beyond the intraseasonal band. In an earlier study, *Zavala-Garay et al.* [2005] emphasized the importance of the low-frequency component of the MJO winds in causing SST changes from a linear point of view. In such a case the SST anomalies in the eastern Pacific can persist long enough for coupling with the atmosphere to occur and thus a possible amplification of SST anomalies. In our MJO run, the input winds are band-pass filtered and hence do not contain variations on longer time scales. As a result, the signals shown in Figure 6b are purely from nonlinear rectification.

5. Summary and Discussion

[36] Sea level and temperature variations associated with the MJO are simulated using a global general circulation model and forcing from a realistic atmospheric reanalysis. The MJO-related sea level and SST changes are also derived from observations, and the model solutions are derived under the full forcing (the CTL run), the realistic wind stress (the WIND run), and the surface buoyancy fluxes (the BUOY run). Comparison of results shows that the CTL run can reproduce the observed spatial distribution of sea level and SST variability (Figures 1 and 3). The MJO-related sea level variations can be mostly accounted for by wind stress forcing (Figure 1). The situation is more complicated for SST: in the Indian Ocean, buoyancy forcing is more important than wind stress; in the eastern tropical Pacific, contributions of buoyancy forcing and wind stress are comparable; in the central tropical Pacific, wind stress is more important than buoyancy forcing (Figure 3).

[37] An additional sensitivity simulation, the MJO run, was carried out to isolate the ocean response to MJO zonal

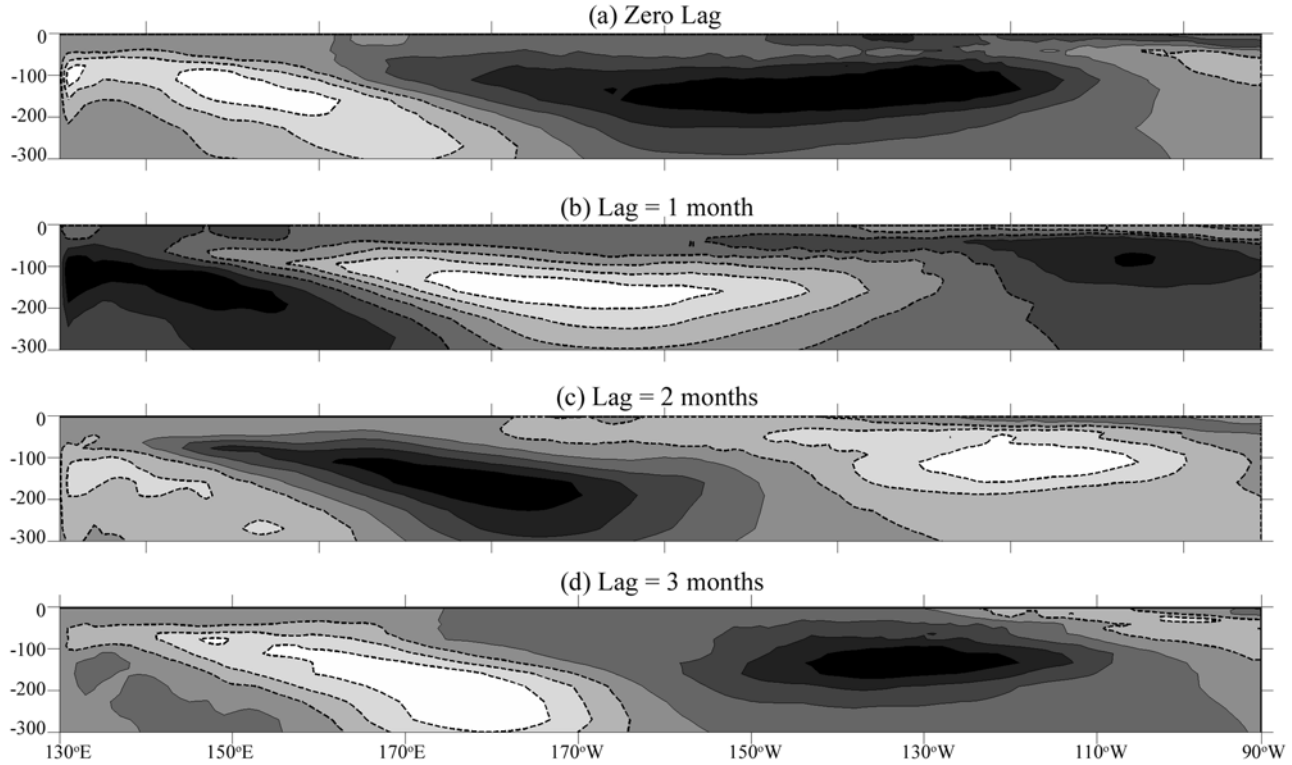

Figure 7. The first mode of the extended empirical orthogonal functions of $T_m - T_b$ in the vertical section along the equator. The time lags are (a) 0, (b) 1, (c) 2, and (d) 3 months. The amplitude of the anomalies is arbitrary with positive (negative) values shown by solid (dashed) lines. Depths are in m.

wind forcing and to better understand the underlying physical mechanisms. Unlike previous studies using idealized or canonical MJO wind forcing [e.g., *Kessler and Kleeman*, 2000; *Waliser et al.*, 2003], the MJO zonal wind used in the present study is extracted from a realistic atmospheric reanalysis. As a result, the model-simulated time series can be directly compared with observations. The ocean response to the MJO zonal wind forcing is quantified

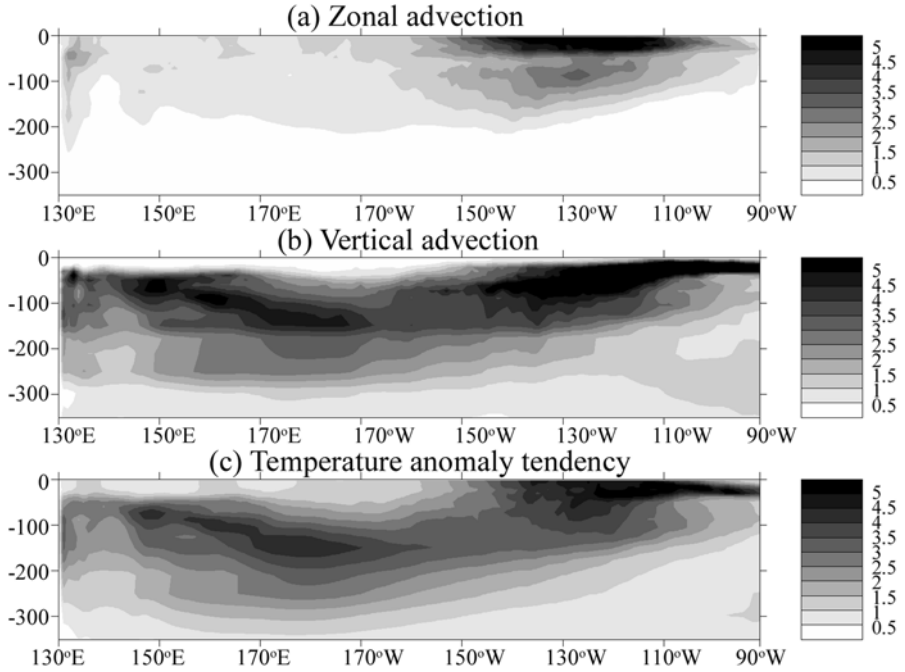

Figure 8. The standard deviation (in 10^{-7} °C s^{-1}) of (a) $u_m \partial T_m/\partial x - u_b \partial T_b/\partial x$, (b) $w_m \partial T_m/\partial z - w_b \partial T_b/\partial z$, and (c) $\partial(T_m - T_b)/\partial t$ in a vertical section along the equator. Depths are in m.

as the difference between the MJO and BUOY runs. Consistent with satellite altimeter observations, the model results show that large sea level variations occur in the equatorial Pacific and Indian Ocean and propagate eastward as baroclinic Kelvin waves (Figure 2). The zonal currents forced by the MJO zonal wind are significant in the western Pacific and eastern Indian oceans, where the MJO wind forcing is strong. The magnitude of the zonal current can reach 0.4 m s^{-1} (Figure 5).

[38] Westerly MJO winds produce a positive subsurface temperature anomaly, while the easterly winds produce a negative anomaly. An EEOF analysis shows that the subsurface temperature anomalies propagate eastward along the thermocline and rise to the surface in the eastern Pacific (Figure 7). The heat budget analysis reveals that the vertical advection plays an important role in the evolution of the subsurface temperature anomalies. Zonal advection makes an important contribution to the SST intraseasonal variations in the central Pacific (Figure 8). *Zhang* [2001] identified a particular pattern of intraseasonal perturbations in SST in the eastern Pacific. The present model results support the argument that modifying the effect of background upwelling associated with MJO-forced Kelvin waves generates these perturbations.

[39] Using observations from five moorings in the equatorial eastern Pacific, *Wang and Weisberg* [2001] examined the influence of ocean circulation on SST and found that vertical advection plays the most important role. The effects of upwelling and downwelling were found to be associated with the SST cooling and warming, respectively. Their observational results are supported by the model results of the present study.

[40] In this study, band-pass filtering and removal of interannual variations primarily associated with ENSO from the MJO index [*Wheeler and Hendon*, 2004] meant that the MJO winds used to force the model do not include low-frequency components. While this limits the discussion of linear response of the ocean to low-frequency MJO forcing [*Zavala-Garay et al.*, 2005], it enables us to quantify the contribution of the nonlinear rectification of the intraseasonal MJO forcing. In a previous study, *Jiang et al.* [2009] examined the rectification over 5 years and could not determine whether rectification of the MJO may have influence on ENSO. In this study, we find that the magnitude of the rectification does vary on interannual time scales and becomes larger during ENSO warm events. The wind forcing used in this study comes from atmospheric reanalysis products, which are thought to be smaller than the more realistic QuikSCAT winds. The rectification in this study is smaller than the previous study of *Jiang et al.* [2009].

[41] The model used in this study is ocean-only, and we focus solely on the impact of MJO zonal winds at low latitudes. Many other processes are potentially important but are not addressed here. Some of these issues can be addressed through modifying the forcing and additional model sensitivity experiments. For example, to examine the influence of the meridional structure of the westerly winds, we could modify the weighting factor used when merging the MJO and climatological winds [*Giese and Harrison*, 1991]. Another possibility is the MJO-related heat forcing; because the MJO and BUOY runs use similar (albeit realistic) input variables for computing surface heat fluxes, the differences between the two runs contain insignificant contributions from intraseasonal heat flux changes. This may explain some of the differences between the CTL run and the differences between the MJO and BUOY runs, as shown in Figure 3. Clearly, additional model sensitivity experiments could be designed to address this issue. In addition to the warming in the central and eastern Pacific, the surface cooling in the western Pacific due to enhanced evaporation and reduced solar radiation associated with the MJO tends to flatten the zonal SST gradient. The change of the zonal SST gradient may cause a large-scale atmospheric feedback, which could potentially further interact with the ENSO cycle. Finally, quantifying the MJO effect on the ENSO is a challenge and will eventually require fully coupled, realistic ocean-atmosphere models. For example, on the basis of an intermediate coupled model, *Kessler and Kleeman* [2000] found that the rectification of the MJO in the western and central Pacific can interact constructively with the ENSO cycle and amplify the warm event by 50%. It will be interesting to further examine the role of the SST rectification signal on low-frequency variations of the coupled system.

Appendix A: Setup of the MJO Run

[42] To construct the zonal wind coherent with the MJO, a band-pass filter with cutoff periods of 20 and 120 days was first performed on the time series of CORE zonal wind velocities between 30°S and 30°N. The MJO indices are then subsampled at the same 6 hourly intervals as the wind fields. Next the wind variations coherent with the MJO were extracted from the band-pass-filtered zonal winds, using the coherency analysis method described at the beginning of section 3, recapping the work by *Zhang et al.* [2009] and *Oliver and Thompson* [2010]. This was achieved by first calculating the Fourier transform of the zonal wind and then multiplying the complex Fourier amplitude by the frequency-dependent transfer functions relating the zonal wind to the MJO indices (RMM1 and RMM2). Applying the inverse Fourier transform then gave the time series of the zonal wind that are perfectly coherent with the MJO. A weighting factor was applied when merging the MJO winds with the climatological winds of NYF. The weighting factor was given by $\exp(-\beta y^2/2c)$, where y is the distance from the equator, β is the meridional gradient of the Coriolis parameter, and c = 2.7 m s^{-1} is the phase speed of the first mode of the baroclinic Kelvin wave. The weighting is consistent with the fact that the MJO signals in wind are confined to a narrow latitudinal band (e.g., 10°N–10°S) and decay away from the equator, in spite of the strong seasonality. Although the weighting factor is symmetrical about the equator, the resulting MJO-related zonal wind can be unsymmetrical.

[43] **Acknowledgments.** X.Z.'s visit at Dalhousie University is supported by the China Scholarship Council and Nanjing University. K.R.T., H.R., and Y.L. acknowledge support from the Global Ocean-Atmosphere Prediction and Predictability research network funded by the Canadian Foundation for Climate and Atmospheric Sciences. J.J. acknowledges support from the National Key Technology R&D Program of China under grant 2009BAC51B01 and the Specialized Research Fund for the Doctoral Program of Higher Education of China under grant 200802840022. We thank Chunzai Wang and an anonymous reviewer for their insightful and constructive comments.

References

Barnier, B., et al. (2006), Impact of partial steps and momentum advection schemes in a global ocean circulation at eddy permitting resolution, *Ocean Dyn.*, *56*, 543–567, doi:10.1007/s10236-006-0082-1.

Belamari, S., J.-L. Redelsperger, and M. Pontaud (2003), Dynamic role of a westerly wind burst in triggering an equatorial Pacific warm event, *J. Clim.*, *16*, 1869–1890, doi:10.1175/1520-0442(2003)016<1869:DROAWW>2.0.CO;2.

Blanke, B., and O. Delecluse (1993), Variability of the tropical Atlantic ocean simulated by a general circulation model with two different mixed-layer physics, *J. Phys. Oceanogr.*, *23*, 1363–1388, doi:10.1175/1520-0485(1993)023<1363:VOTTAO>2.0.CO;2.

Enfield, D. B., and R. Lukas (1983), Low-frequency sea level variability along the South American coast in 1981–83, *Trop. Ocean Atmos. Newsl.*, *28*, 2–4.

Fichefet, T., and M. A. Morales Maqueda (1997), Sensitivity of a global sea ice model to the treatment of ice thermodynamics and dynamics, *J. Geophys. Res.*, *102*, 12,609–12,646, doi:10.1029/97JC00480.

Gent, P. R., and J. C. McWilliams (1990), Isopycnal mixing in ocean circulation models, *J. Phys. Oceanogr.*, *20*, 150–155, doi:10.1175/1520-0485(1990)020<0150:IMIOCM>2.0.CO;2.

Giese, B. S., and D. E. Harrison (1991), Eastern equatorial Pacific response to three composite westerly wind types, *J. Geophys. Res.*, *96*, suppl., 3239–3248.

Gill, A. E. (1975), Models of equatorial currents, in *Numerical Models of Ocean Circulation: Proceedings of a Conference*, pp. 181–203, Natl. Acad. of Sci., Washington, D. C.

Gille, S. T. (2005), Statistical characterization of zonal and meridional ocean wind stress, *J. Atmos. Oceanic Technol.*, *22*, 1353–1372, doi:10.1175/JTECH1789.1.

Han, W., D. M. Lawrence, and P. J. Webster (2001), Dynamical response of the equatorial Indian Ocean to intraseasonal winds: Zonal flow, *Geophys. Res. Lett.*, *28*, 4215–4218, doi:10.1029/2001GL013701.

Hendon, H. H. (2005), Air-sea interaction, in *Intraseasonal Variability in the Atmosphere-Ocean System*, edited by W. K. M. Lau and D. E. Waliser, pp. 223–246, doi:10.1007/3-540-27250-X_7, Springer, Berlin.

Hsu, H.-H. (1996), Global view of the intraseasonal oscillation during northern winter, *J. Clim.*, *9*, 2386–2406, doi:10.1175/1520-0442(1996)009<2386:GVOTIO>2.0.CO;2.

Jiang, C., L. Thompson, K. Kelly, and M. F. Cronin (2009), The roles of intraseasonal Kelvin waves and tropical instability waves in SST variability along equatorial Pacific in an isopycnal ocean model, *J. Clim.*, *22*, 3470–3487, doi:10.1175/2009JCLI2767.1.

Jones, C., D. E. Waliser, and C. Gautier (1998), The influence of the Madden-Julian Oscillation on ocean surface heat fluxes and sea surface temperature, *J. Clim.*, *11*, 1057–1072, doi:10.1175/1520-0442(1998)011<1057:TIOTMJ>2.0.CO;2.

Kessler, W. S. (2001), EOF representations of the Madden-Julian Oscillation and its connection with ENSO, *J. Clim.*, *14*, 3055–3061, doi:10.1175/1520-0442(2001)014<3055:EROTMJ>2.0.CO;2.

Kessler, W. S. (2005), The oceans, in *Intraseasonal Variability in the Atmosphere-Ocean System*, edited by W. K. M. Lau and D. E. Waliser, pp. 175–222, doi:10.1007/3-540-27250-X_6, Springer, Berlin.

Kessler, W. S., and R. Kleeman (2000), Rectification of the Madden-Julian Oscillation into the ENSO cycle, *J. Clim.*, *13*, 3560–3575, doi:10.1175/1520-0442(2000)013<3560:ROTMJO>2.0.CO;2.

Large, W. G., and S. G. Yeager (2004), Diurnal to decadal global forcing for ocean and sea-ice models: The data sets and flux climatologies, *NCAR Tech. Note, NCAR/TN-460+STR*, 111 pp.

Madden, R. A., and P. R. Julian (1994), Observations of the 40–50 day tropical oscillation—A review, *Mon. Weather Rev.*, *122*, 814–847, doi:10.1175/1520-0493(1994)122<0814:OOTDTO>2.0.CO;2.

Madec, G., P. Delecluse, M. Imbard, and C. Levy (1998), OPA 8.1 ocean general circulation model reference manual, *Notes LPSL 11*, 91 pp., Univ. Pierre et Marie Curie, Paris.

McPhaden, M. J. (2002), Mixed layer temperature balance on intraseasonal timescales in the equatorial Pacific Ocean, *J. Clim.*, *15*, 2632–2647, doi:10.1175/1520-0442(2002)015<2632:MLTBOI>2.0.CO;2.

Moore, A. M., and R. Kleeman (1999), Stochastic forcing of ENSO by the intraseasonal oscillation, *J. Clim.*, *12*, 1199–1220, doi:10.1175/1520-0442(1999)012<1199:SFOEBT>2.0.CO;2.

Oliver, E., and K. R. Thompson (2010), Madden-Julian Oscillation and sea level: Local and remote forcing, *J. Geophys. Res.*, *115*, C01003, doi:10.1029/2009JC005337.

Picaut, J., F. Masia, and Y. D. Penhoat (1997), An advective-reflective conceptual model for the oscillatory nature of the ENSO, *Science*, *277*, 663–666, doi:10.1126/science.277.5326.663.

Reynolds, R. W., and T. M. Smith (1994), Improved global sea surface temperature analyses using optimum interpolation, *J. Clim.*, *7*, 929–948, doi:10.1175/1520-0442(1994)007<0929:IGSSTA>2.0.CO;2.

Roundy, P. E., C. J. Schreck, and M. A. Janiga (2009), Contributions of convectively coupled equatorial Rossby waves and Kelvin waves to the real-time multivariate MJO indices, *Mon. Weather Rev.*, *137*, 469–478, doi:10.1175/2008MWR2595.1.

Shinoda, T., and H. H. Hendon (2001), Upper-ocean heat budget in response to the Madden-Julian Oscillation in the western equatorial Pacific, *J. Clim.*, *14*, 4147–4165, doi:10.1175/1520-0442(2001)014<4147:UOHBIR>2.0.CO;2.

Shinoda, T., H. H. Hendon, and J. Glick (1998), Intraseasonal variability of surface fluxes and sea surface temperature in the tropical Indian and Pacific oceans, *J. Clim.*, *11*, 1685–1702, doi:10.1175/1520-0442(1998)011<1685:IVOSFA>2.0.CO;2.

Slingo, J. M., D. P. Rowell, K. R. Sperber, and E. Nortley (1999), On the predictability of the interannual behavior of the Madden-Julian Oscillation and its relationship with El Nino, *Q. J. R. Meteorol. Soc.*, *125*, 583–609.

Smith, W. H. F., and D. T. Sandwell (1997), Global seafloor topography from satellite altimetry and ship depth soundings, *Science*, *277*, 1956–1962, doi:10.1126/science.277.5334.1956.

Waliser, D. E., R. Murtugudde, and L. E. Lucas (2003), Indo-Pacific Ocean response to atmospheric intraseasonal variability: 1. Austral summer and the Madden-Julian Oscillation, *J. Geophys. Res.*, *108*(C5), 3160, doi:10.1029/2002JC001620.

Wang, C., and R. H. Weisberg (2001), Ocean circulation influences on the sea surface temperature in the equatorial central Pacific, *J. Geophys. Res.*, *106*, 19,515–19,526, doi:10.1029/2000JC000242.

Weare, B. C., and J. S. Nasstrom (1982), Examples of extended empirical orthogonal function analyses, *Mon. Weather Rev.*, *110*, 481–485, doi:10.1175/1520-0493(1982)110<0481:EOEEOF>2.0.CO;2.

Wheeler, M. C., and H. H. Hendon (2004), An all-season real-time multivariate MJO Index: Development of an index for monitoring and prediction, *Mon. Weather Rev.*, *132*, 1917–1932, doi:10.1175/1520-0493(2004)132<1917:AARMMI>2.0.CO;2.

Zavala-Garay, J., C. Zhang, A. M. Moore, and R. Kleeman (2005), The linear response of ENSO to the Madden-Julian Oscillation, *J. Clim.*, *18*, 2441–2459, doi:10.1175/JCLI3408.1.

Zavala-Garay, J., C. Zhang, A. M. Moore, A. T. Wittenberg, M. J. Harrison, A. Rosati, J. Vialard, and R. Kleeman (2008), Sensitivity of hybrid ENSO models to unresolved atmospheric variability, *J. Clim.*, *21*, 3704–3721, doi:10.1175/2007JCLI1188.1.

Zhang, C. (2001), Intraseasonal perturbations in sea surface temperatures of the equatorial eastern Pacific and their association with the Madden-Julian Oscillation, *J. Clim.*, *14*, 1309–1322, doi:10.1175/1520-0442(2001)014<1309:IPISST>2.0.CO;2.

Zhang, C., and J. Gottschalck (2002), SST anomalies of ENSO and the Madden-Julian Oscillation in the equatorial Pacific, *J. Clim.*, *15*, 2429–2445, doi:10.1175/1520-0442(2002)015<2429:SAOEAT>2.0.CO;2.

Zhang, C., and M. J. McPhaden (2000), Intraseasonal surface cooling in the equatorial western Pacific, *J. Clim.*, *13*, 2261–2276, doi:10.1175/1520-0442(2000)013<2261:ISCITE>2.0.CO;2.

Zhang, X., Y. Lu, and K. Thompson (2009), Sea level variations in the tropical Pacific Ocean and the Madden-Julian Oscillation, *J. Phys. Oceanogr.*, *39*, 1984–1992, doi:10.1175/2009JPO4170.1.

J. Jiang and X. Zhang, School of Atmospheric Sciences, Nanjing University, Nanjing, Jiangsu 210093, China.

Y. Lu, Ocean Sciences Division, Fisheries and Oceans Canada, Bedford Institute of Oceanography, 1 Challenger Dr., Dartmouth, NS B2Y 4A2, Canada. (LuY@mar.dfo-mpo.gc.ca)

H. Ritchie, Meteorological Research Division, Environment Canada, 2121 Trans-Canada Hwy., Dorval, QC H9P 1J3, Canada.

K. R. Thompson, Department of Oceanography, Dalhousie University, 1355 Oxford St., Hallifax, NS B3H 4J1, Canada.